applied sciences

MDPI

Article

Electrochemical Performance of Ti Gr. 2 as Electrodes in Contact with Saline Suspension of Clays during the Electroflotation Process

Alvaro Soliz [1,*], Felipe M. Galleguillos-Madrid [2,*], José Ángel Cobos-Murcia [3], Sebastian Angulo [2], Sebastian Salazar-Avalos [2], Bernabé Alonso-Fariñas [4] and Alexis Guzmán [1]

[1] Departamento de Ingeniería en Metalurgia, Universidad de Atacama, Av. Copayapu 485, Copiapó 1530000, Chile; alexis.guzman@uda.cl
[2] Centro de Desarrollo Energético Antofagasta, Universidad de Antofagasta, Antofagasta 1240000, Chile; sebastian.angulo.araya@ua.cl (S.A.); sebastian.salazar@uantof.cl (S.S.-A.)
[3] Instituto de Ciencias Básicas e Ingeniería, Universidad Autónoma del Estado de Hidalgo, Carr. Pachuca-Tulancingo km. 4.5, Mineral de la Reforma 42184, Hidalgo, Mexico; jose_cobos@uaeh.edu.mx
[4] Departamento de Ingeniería Química y Ambiental, Escuela Técnica Superior de Ingeniería, Universidad de Sevilla, Camino de los Descubrimientos s/n, 41092 Sevilla, Spain; bernabeaf@us.es
* Correspondence: alvaro.soliz@uda.cl (A.S.); felipe.galleguillos.madrid@uantof.cl (F.M.G.-M.)

Abstract: The presence of clays in copper minerals has a significant negative impact during their processing, leading to low recoveries during the flotation process. In saline environments, the presence of these clays promotes operational problems associated with salinity, leading to decreases in the copper concentrate grade, alterations in the rheology of the mineral pulp, reduction in the selectivity of copper during the flotation process, declines in the quality of clarified water, and excessive corrosion of metallic components. This study explores the electroflotation of kaolinite and montmorillonite clays in NaCl solutions using a modified Hallimond tube coupled with Ti Gr. 2 electrodes for bubble generation via water electrolysis and the corrosion analysis of these electrodes applying the superposition model. The electroflotation results show recovery of clays close to 72.68% for kaolinite, 88.44% for montmorillonite, and 67.36% for a mixture of both clays. The presence of clays helps reduce the corrosive effects of Ti Gr. 2 from 0.069 A/m^2 in NaCl to 0.0073 A/m^2 in NaCl with montmorillonite clay.

Keywords: kaolinite clay; montmorillonite clay; electroflotation; titanium Gr. 2 electrode; superposition model

Citation: Soliz, A.; Galleguillos-Madrid, F.M.; Cobos-Murcia, J.Á.; Angulo, S.; Salazar-Avalos, S.; Alonso-Fariñas, B.; Guzmán, A. Electrochemical Performance of Ti Gr. 2 as Electrodes in Contact with Saline Suspension of Clays during the Electroflotation Process. *Appl. Sci.* **2024**, *14*, 8825. https://doi.org/10.3390/app14198825

Academic Editor: Angeles Sanroman Braga

Received: 29 July 2024
Revised: 29 August 2024
Accepted: 6 September 2024
Published: 1 October 2024

1. Introduction

Overexploitation of water sources in hyper-arid and arid regions, such as northern Chile, southern Peru, northern China, and parts of Africa, Asia, and Australia, has led to water scarcity, necessitating the search for new sources and better water management practices [1–3]. While mining globally uses a relatively small amount of water, it can be a significant consumer at the local level. In Chilean mining, approximately 3% of the total available water is utilized, drawn from three primary sources: continental water, seawater, and recirculated water. Continental water is sourced from underground aquifers, lakes, rivers, and wetlands. Seawater undergoes desalination by private entities and is then pumped to mining sites. Data from COCHILCO indicate that the use of continental water in 2022 decreased by 10.8% compared to its use in 2018 [4]. However, the use of this source has come under scrutiny due to its dwindling availability and increasing demand, prompting a shift towards seawater usage in mining operations over the years. Regarding continental water usage in mining, we can identify five primary areas: concentration processes, which emerge as the most water-intensive, consuming 74.3% of available resources; hydrometallurgy, which follows closely behind at 10.2%; the mining phase, which

accounts for over 5.6% of water usage; smelting and refining operations, which utilize 3.6% of the total water volume; and other uses, including supply to third parties, accounting for 6.3% [4]. In all these cases, the reuse of water is a priority for the sustainability of the process. However, the recirculated water, used to minimize the consumption of freshwater, typically carries lower quality, containing dissolved waste and colloidal particles, such as dissolved components and especially clays, generating a negative effect on the process [5].

Clays are usually dispersed in mineral slurries as ultrafine particles, creating conditions for the slurry to behave as a non-Newtonian fluid that affects the entire mineral processing chain. In particular, the efficiency of flotation of copper sulfides is severely impacted by clay minerals. The long-term stability of clay colloidal particles in the electrolyte presents significant challenges in mineral processing due to the low shear strength of discarded solids in mineral operations, such as tailings, reduced consolidation and strength gain over time, and difficulties in water recovery during subsequent ore processing. These types of minerals can be separated by sedimentation and/or flotation processes, but ultrafine clays pose a challenge for mineral processing due to physical properties such as particle size, shape, and density. Parameters such as those mentioned are critical for understanding the behavior of these particles in saline solutions like seawater. The presence of soluble salts can disrupt the stability of clay colloids, enhancing sedimentation and consolidation, promoting strength gain, and improving water recovery. Increased water salinity improves the volume of froth floating by diminishing settling [6]. Particle weight is the dominant force that governs the behavior of coarse clay particles in suspension, whereas inter-particle forces, due to the small particle size and high specific surface area, primarily dominate the behavior of fine-grained particles. It has been reported that the aggregation rate of nano-sized clay particles present in oil sand tailings increases with rising NaCl concentration and that the initial settling rate of oil sand tailings increases with higher pH and/or the presence of divalent cations (Ca^{2+} and Mg^{2+}) [7].

The presence of clay significantly hampers copper ore flotation, leading to decreased recovery rates and a subsequent decline in concentrate grades. Clays are classified as swelling and non-swelling based on their water-absorption capabilities. Kaolinite is a non-swelling clay with the general composition $Al_2Si_2O_5(OH)_4$, which has features that lie in the prevalence of Al^{3+} in its octahedral sites, where isomorphic substitutions occur with Mg^{2+}, Fe^{3+}, V^{3+}, and Ti^{4+} [8]. Montmorillonite is a welling clay with the general composition $(Na, Ca)_{0.3}(Al, Mg)_2Si_4O_{10}(OH)_2.n(H_2O)$, with a nanolayered structure consisting of stacked layers about 1 nm thick [9]. In mineral processing, kaolinite presents numerous challenges, including increased fines during size reduction stages (reaching sizes < 20 μm), interfering with the flotation process by affecting bubble stability, altering foam rheology, compromising the selectivity of valuable ore recovery, and reducing the quality of recirculated water, particularly at alkaline pH levels (pH > 8), resulting in the accumulation of suspended particles. On the other hand, due to the small particle size of montmorillonite clay and its high charge density, this clay poses challenges in mineral processing because it tends to remain suspended in solution. In the presence of montmorillonite, it is crucial to adjust the solution ionic strength to avoid significant swelling and eventual disintegration of the clay. Notably, the abundance of Cl^- ions and multivalent cations (Al^{3+}, Ca^{2+}, Mg^{2+}, K^+, and Na^+) in the electrolyte notably enhances the natural sedimentation of montmorillonite compared to their performance in pure water due to an increase in the ionic strength.

A technique to improve water quality in the presence of clay particles is the application of the electroflotation process. This method employs an electrochemical approach to effectively eliminate suspended particles such as colloids, microalgae, or oil from seawater, often serving as a preliminary treatment step. A widespread use of this method is in municipal water treatment and the removal of microalgae or metal ions from municipal wastewater [10–16]. Despite these advancements, there remains limited research in the scientific literature related to the use of electroflotation with seawater in the mining industry [17,18]. Specifically, there is a lack of research on its efficacy in removing ultrafine mineral particles

such as clays, pyrite [19], chalcopyrite [20,21], hematite [22], and other minerals [23–25]. The liquid–solid separation by electroflotation involves lifting ultrafine particles of clay to the water surface through microbubbles of H_2 and O_2 generated by the seawater splitting process via cathodic and anodic reactions [17,26]. The electroflotation process offers several key advantages, notably the absence of chemical additives and the ability to regulate bubble density within the reactor by adjusting the applied potential. The literature reveals that the electroflotation process is successfully applied in the recovery of fine and ultrafine particles compared to other conventional techniques such as froth flotation, ion flotation, solvent sublation, or absorbing colloid flotation. This effectiveness is mainly attributed to the production of smaller particle sizes, ranging between 5 and 50 μm depending on the application, uniform bubble-particle formation, and high-frequency production, which can also be manipulated by varying operational variables such as pH, current density, type of electrodes, and others [18,27]. The application of electroflotation for clay removal in high salinity solutions like seawater (~0.5 M NaCl) has not been deeply studied.

Corrosion in saline environments poses a significant threat to the durability and effectiveness of equipment used in electroflotation processes, ultimately impacting operational costs. By understanding the corrosion mechanisms inherent in salt electroflotation, we can make informed decisions regarding material selection for equipment construction under aggressive conditions. This proactive approach not only extends the equipment's lifespan but also reduces maintenance expenses while preserving its mechanical integrity. Moreover, corrosion directly alters the properties of electrodes by modifying their surfaces and affecting other components of the electrochemical device [28]. This can lead to a decline in the flotation and recovery capacity of clays, further emphasizing the critical importance of addressing corrosion issues in saline electroflotation environments. The efficiency of ultrafine particle removal via electroflotation hinges on a series of surface electrode reactions and the inherent stability of particles, influenced by their hydrophobicity [17,25].

This work studies the electroflotation of kaolinite and montmorillonite clays, as well as their mixture, in a 0.5 M NaCl solution using Ti Gr. 2 electrodes as anode and cathode. The flotation process was conducted using a modified Hallimond tube-electroflotation device across a salinity range of 0.1 to 0.5 M of NaCl under different cell voltage and electroflotation times. Additionally, corrosion studies of the Ti Gr. 2 electrode in the clay slurries were carried out using the potentiodynamic polarization technique. This study significantly contributes to the understanding of the electroflotation process of saline clay slurries and the corrosion behavior through the use of mixed potential theory.

2. Materials and Methods

2.1. Electroflotation System

The electroflotation tests were conducted using a modified Hallimond tube, specifically tailored for investigating conventional flotation processes. The Hallimond tube comprises an upper section featuring an angled tube that facilitates the ascent of the floated material to the surface, complemented by a conical receiver designed to capture the floated mass. At the base, provisions are made for air inlet and outlet for non-floated fractions. This bottom section was modified to accommodate an electrical component, housing connecting cables directly linked to the power source and electrodes, supplemented with rubber bands to insulate the electrolyte from the cables. This adaptation effectively repurposes the apparatus originally intended for air inflow, facilitating the generation of bubbles from the base. The cell used in this work had a volume of 250 cm^3 with two cylindrical electrodes of 4.4 cm^2 of Titanium Gr. 2 (Ti Gr. 2), obtained from Balance World Inc. (Putian, China), as shown in Figure 1.

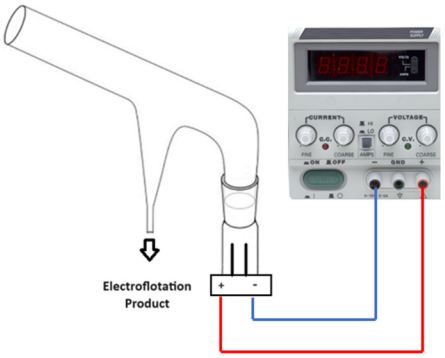

Figure 1. Diagram of the modified Hallimond tube used for the electroflotation tests.

2.2. Materials and Solutions

The montmorillonite and kaolinite samples, sourced from Science Words (Los Angeles, CA, USA), underwent comprehensive characterization using cutting-edge techniques such as scanning electron microscopy (SEM) and energy-dispersive X-ray (EDS) analyzers (Hitachi SU 500, Hitachi, Japan, and Zeiss EVO MA 10, Jena, Germany), and X-ray diffraction (XRD) (Bruker Advance D8, Billerica, MA, USA). Test solutions of concentrations 0.1, 0.3, and 0.5 M NaCl were meticulously prepared using NaCl (analytical grade) and deionized water. The solution pH was adjusted by adding drops of 1 M NaOH. All chemicals were purchased from Merck (Merck, Providencia, Chile).

2.3. Electroflotation Tests

For the electroflotation experiments, three different synthetic saline slurries were prepared: 1 g/L of kaolinite, 1 g/L of montmorillonite, and 1 g/L of the mixture 1:1 of both clays, considering concentrations of 0.1, 0.3, and 0.5 M of NaCl. The particle sizes of kaolinite and montmorillonite were equivalent to a −635 mesh Tyler with a d_{80} of 5 µm. All electroflotation experiments were carried out at room temperature of 19 ± 0.5 °C and atmospheric pressure. The power supply was connected to the anode and cathode, operating at fixed cell voltages (E_{cell}) of 10, 15, and 20 V, with electroflotation times of 10, 15, and 20 min.

Colloidal suspension preconditioning was performed in an agitator tank for 30 min at 500 rpm at a fixed pH of 8. Subsequently, for electroflotation, NaCl solutions were homogenized for 15 min at 700 rpm using a magnetic stirrer. The suspension was promptly transferred to the Hallimond cell to perform electroflotation studies. Upon completion of the electroflotation experiment, the floated product was thoroughly extracted using a peristaltic pump and then collected in a beaker. The collected product was then filtered using a vacuum pump connected to a Büchner funnel and dried in a universal oven at 105 °C for 24 h. Finally, the mass of dried clay particles was weighted on an analytical scale. The electroflotation efficiency R_{MF} was determined using the following equation:

$$R_{MF} = \frac{m_f}{m_i} \cdot 100\% \quad (1)$$

where m_i is the initial mass of clay fed to the modified Hallimond cell, and m_f is the total mass recovered after the electroflotation experiments, including Ti flocs and clays.

2.4. Electrochemical and Corrosion Studies for Ti Gr. 2

The electrochemical and corrosion behavior of Ti Gr. 2 in 0.5 M NaCl solutions, both with and without clays, were studied with a focus on the hydrogen evolution reaction (HER), oxygen reduction reaction (ORR), and titanium oxidation reaction (TOR) as the main electrochemical partial reactions [29–34]. Potentiodynamic polarization measurements were conducted using Ti Gr. 2 working electrodes connected to a rotating disk electrode interface. These working electrodes were small cylindrical bars, with 4 mm in diameter

and 10 mm in length, which were embedded concentrically into a PTFE tube with an 8 mm diameter and sealed with epoxy adhesive resin. Before potentiodynamic measurements, the electrodes were abraded and polished successively with silicon carbide sandpaper from 600 to 1200 mesh. The experiments were carried out in triplicate at a temperature of 20 ± 0.5 °C by circulating hot water through a jacket cell. All potentials reported are referred to the standard hydrogen electrode (SHE).

A BASI/RDE-2 rotating electrode interface connected to an Epsilon potentiostat/galvanostat (Basi, IN, USA) was used for electrochemical measurements. Platinum wire as a counter electrode and Ag/AgCl (4 M KCl Sat.) as a reference electrode were used. Potentiodynamic polarization measurements were performed in a conventional 3-electrode cell following the methodology reported in previous works [32,35] and covering a potential range between −1100 and 200 mV/SHE at a scan rate of 2 mV/s. The rotation electrode for the Ti Gr. 2 was 1200 rpm.

2.5. Kinetic Corrosion Analysis

Corrosion of pure titanium can produce several anodic and cathodic reactions, including Ti species that interact with hydrogen protons and hydroxide ions depending on the solution pH [29,31,32,36]. In this work, the corrosion kinetic investigation was conducted utilizing non-linear fitting applied to experimental potentiodynamic curves, employing the superposition model based on mixed potential theory. This approach aligns with the methodology outlined in our prior research, where the total current density can be expressed as follows [32,35,37]:

$$i = i_{O_2} + i_{H_2} + i_{Ti} \quad (2)$$

where i represents the total current density; i_{O_2} and i_{H_2} denote the partial reduction current densities for ORR and HER, respectively; and i_{Ti} denotes the partial oxidation current density for TOR. Although direct experimental measurements of i_{O_2}, i_{H_2}, and i_{Ti} are not feasible, their values can be deduced using a fitting methodology to determine the kinetic parameters of each reaction.

To achieve this, the electrochemical reactions of TOR and HER are considered to be controlled by charge transfer kinetics, while the ORR is controlled by a mixed-charge diffusion mechanism, according to the following expressions [35]:

$$i_{H_2} = i_{0,H_2} \times exp\left(-\frac{2.303 \times \eta_{H_2}}{t_{H_2}}\right) \quad (3)$$

$$i_{O_2} = i_{0,O_2} \times exp\left(-\frac{2.303 \times \eta_{O_2}}{t_{O_2}}\right) \times \left(1 + \frac{i_{0,O_2} \times exp\left(-\frac{2.303 \times \eta_{O_2}}{t_{O_2}}\right)}{i_{l,O_2}}\right)^{-1} \quad (4)$$

$$i_{Ti} = i_{0,Ti} \times exp\left(\frac{2.303 \times \eta_{Ti}}{t_{Ti}}\right) \quad (5)$$

where the $\eta_{O_2} = E - E_{eq,O_2}$, $\eta_{H_2} = E - E_{eq,H_2}$, and $\eta_{Ti} = E - E_{eq,Ti}$ are the ORR, HER, and TOR overpotentials, respectively; i_{0,O_2}, i_{0,H_2}, and $i_{0,Ti}$ are the exchange current densities for ORR, HER, and TOR, respectively; i_{l,O_2} is the limiting current density for ORR; t_{O_2}, t_{H_2}, and t_{Ti} are the Tafel slopes for ORR, HER, and TOR, respectively; and E_{eq,O_2}, E_{eq,H_2}, and $E_{eq,Ti}$ are the equilibrium potentials which are equal to 752 mV, −479 mV, and −1804 mV for ORR, HER, and TOR, respectively, assuming that the main anodic reaction is $Ti \rightarrow Ti^{2+} + 2e^-$ [34]. The root mean square error (RMSE) was used to evaluate the quality of curve fitting.

3. Results

3.1. Mineralogical Characterization of Clays

Figure 2 shows morphological patterns of kaolinite and montmorillonite clays as received. For montmorillonite samples (Figure 2a,c), the morphology consists of grains

with a flat shape and irregular edges, with particle sizes of 5 µm. Conversely, for kaolinite clay (Figure 2b,d), the morphology consists of a structure of silicate sheets joined together with layers of irregular edges, approximately 1 µm in length. Kaolinite presents particles of uniform composition and size, suggesting a more homogeneous structure compared to montmorillonite.

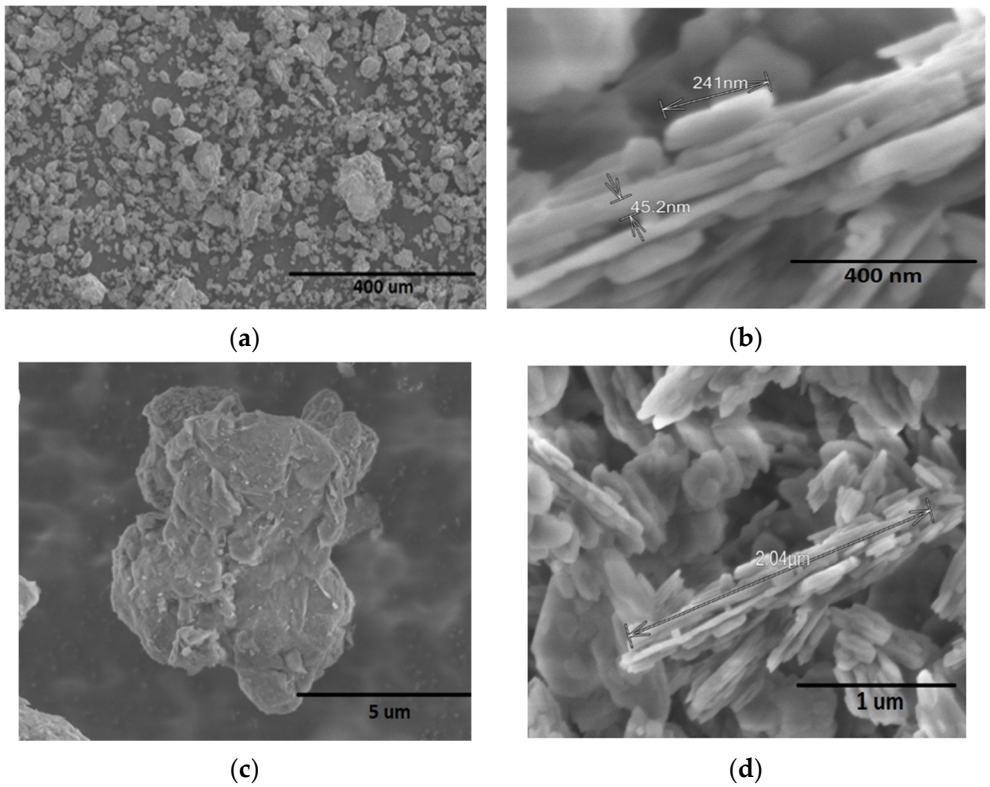

Figure 2. SEM images of (**a**,**c**) montmorillonite and (**b**,**d**) kaolinite clays.

Figure 3 shows images of the elemental analysis for both kaolinite and montmorillonite clays, and Table 1 presents their chemical composition expressed in weight percent (%). For kaolinite clay (Figure 3a), silicon is the predominant element constituting it, followed by aluminum, with a minor presence of iron and titanium. On the other hand, montmorillonite clay (Figure 3b) exhibits a higher percentage of silicon compared to aluminum, where the sample also contains significant amounts of calcium, magnesium, and minor amounts of sodium. These compositions reflect the distinct mineralogical characteristics of kaolinite and montmorillonite, providing insights into their potential effects and behaviors in mineral processing applications.

Table 1. Chemical composition of kaolinite and montmorillonite clays.

Elements	Kaolinite, wt%	Montmorillonite, wt%
Fe	2.47	-
Al	44.53	21.71
Si	48.57	67.48
Ti	4.44	-
Na	-	0.83
Mg	-	1.81
S	-	1.91
Ca	-	6.25

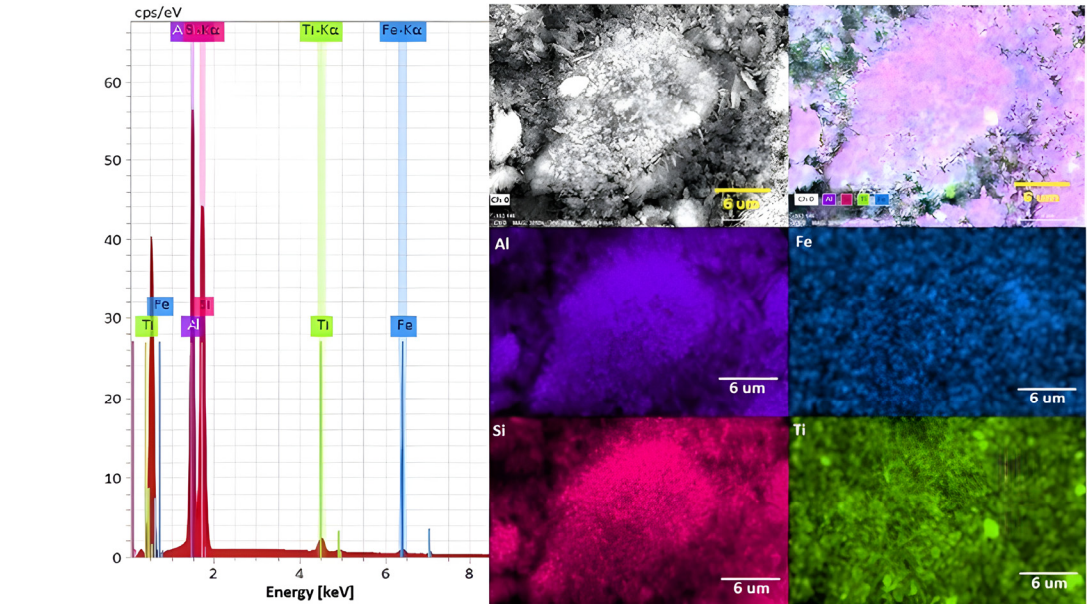

(**a**)

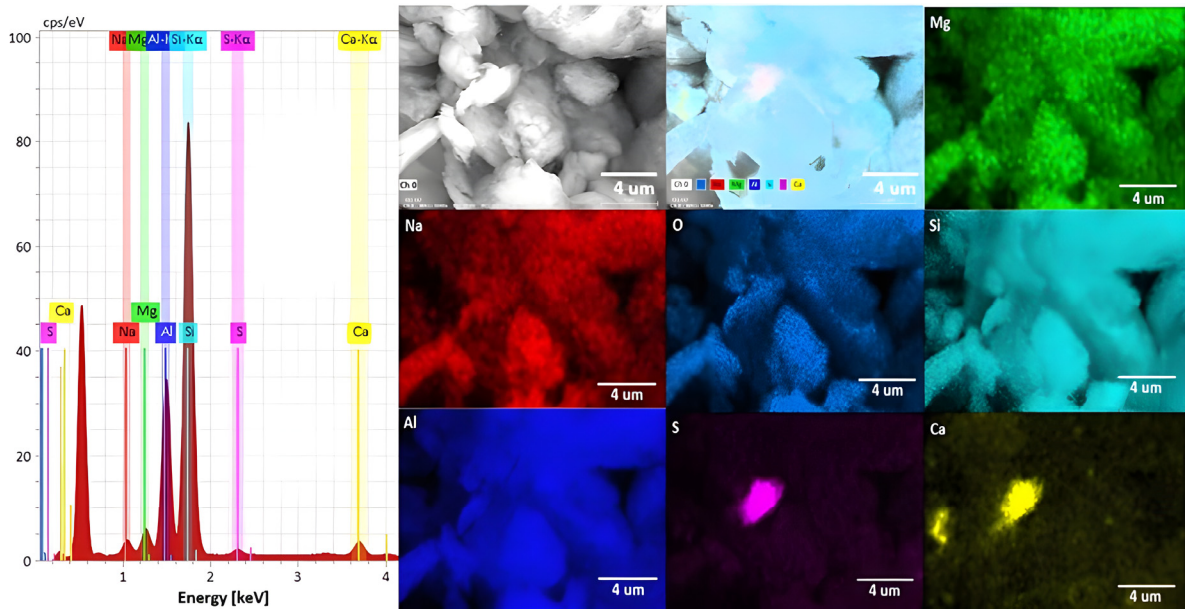

(**b**)

Figure 3. Elemental mapping by EDS analysis of (**a**) kaolinite and (**b**) montmorillonite clays.

XRD analysis was performed to obtain comprehensive characterization of kaolinite and montmorillonite samples, providing valuable insights into their mineralogical composition as shown in Figure 4. The patterns have been analyzed based on Powder Diffraction File (PDF) cards. For the montmorillonite sample (Figure 4a), the results exhibited signals associated with quartz (SiO_2) (PDF: 05-0490) and three forms of montmorillonite: montmorillonite with a phase composed by $MgOAl_2O_35SiO_2 \cdot xH_2O$ (PDF: 03-0014), montmorillonite with sodium content composed by $Na_x(Al, Mg)_2Si_4O_{10}(OH)_2 \cdot zH_2O$ (PDF: 12-0204), and montmorillonite with calcium content composed by $Ca_{0.2}(Al, Mg)_2Si_4O_{10}(OH)_2 \cdot 4H_2O$ (PDF: 13-0135). Conversely, XRD analysis for the kaolinite sample (Figure 4b) displayed patterns and signals corresponding specifically to kaolinite (PDF: 89-6538) and other minor phases such as quartz (SiO_2), magnetite (Fe_3O_4), anatase (TiO_2), and rutile (TiO_2). Kaolinite and montmorillonite, despite their similar phyllosilicate structures, exhibit distinct compositions and morphologies that can significantly impact processing efficiency. In

mineral processing operations, the presence of these clays plays a significant role where several challenges such as increased fines, compromised flotation selectivity, and water quality degradation are observed. Kaolinite's ability to reach ultrafine sizes and interfere with bubble movement exacerbates these issues, while its chemical composition, mainly aluminum and silicon, influences its interactions with other minerals and chemicals. Furthermore, montmorillonite, with its diverse elemental composition including calcium, magnesium, and sodium, introduces additional hurdles due to its complex interactions with processing elements, suggesting potential interactions that may influence flotation behavior, rheological properties, and water quality. Understanding the mineralogical composition and elemental distribution of these clays is crucial for developing tailored strategies to optimize processing efficiency and minimize environmental impacts. Further research into clay–mineral interactions promises innovative solutions to address these challenges effectively.

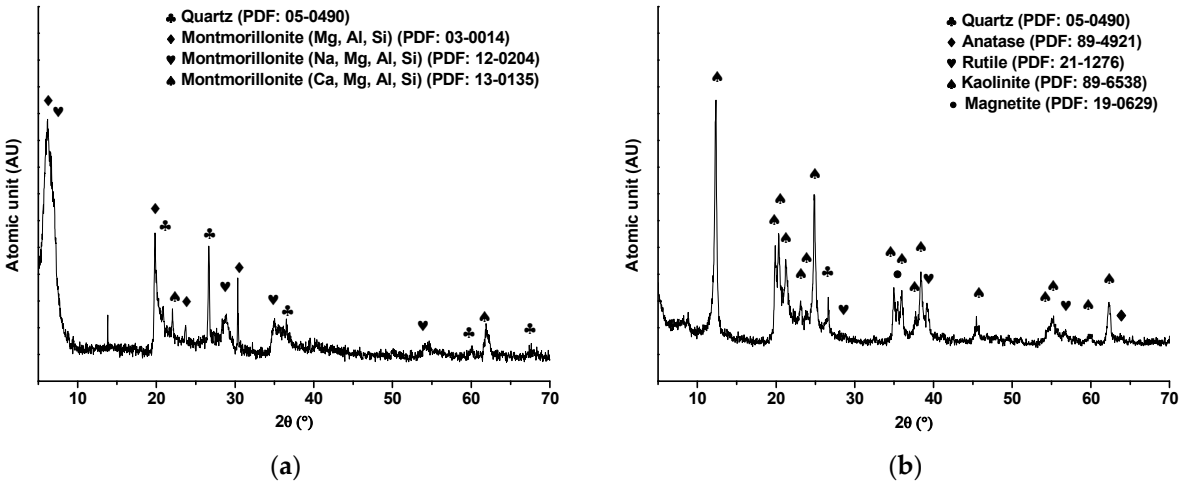

Figure 4. XRD patterns of (**a**) montmorillonite and (**b**) kaolinite clays.

3.2. Electroflotation of Clays in NaCl Solutions

The electroflotation process was performed using a modified Hallimond tube with a pair of cylindrical Ti Gr. 2 electrodes, which were connected from the bottom of the device to a variable power supply as shown in Figure 1. The parameter employed to assess the water quality treated by these electrochemical methods is the electroflotation efficiency (Equation (1)). Figure 5 shows images of the slurries before and after the electroflotation process. In the figure, it is possible to observe the changes in the solution appearance, where a large part of the clays was separated.

During the electroflotation process, the produced foam revealed a sticky consistency, which is a characteristic inherent to clays when they are in contact with aqueous mediums. Through experiments employing applied cell potentials of 10, 15, and 20 V over durations of 10, 15, and 20 min, it was observed that the current intensity varies significantly, as does the amount of clay recovered over time, reaching a steady-state value close to 0.04 A at the end of the electroflotation process, as is tabulated in Table 2. Under these electroflotation conditions, no notable difference was observed in the cell current at the end of the process. However, changes in this variable could be attributed to several factors, including variations in the solution chemistry due to the presence of multiple ions such as Al^{+3}, Fe^{+2}, Fe^{+3}, Mg^{+2}, and Na^{+1}, which come from the dissolution of kaolinite and montmorillonite clays due to their solubility [38]. Additionally, the cell current intensity can be affected by the reduction in the number of active sites on the anodic electrode surface and near the solid–liquid interface, caused by the oxidation of the anodic electrode and further formation of a passive

film composed mainly of TiO_2, following the sequence of electrochemical and chemical reactions [39]:

$$Ti \overset{-2e^-}{\rightarrow} Ti^{2+} \overset{-e^-}{\rightarrow} Ti^{3+} \overset{-e^-}{\rightarrow} Ti^{4+} \quad (6)$$

$$Ti^{4+} + 4OH^- \rightarrow TiO_2 + 2H_2O \quad (7)$$

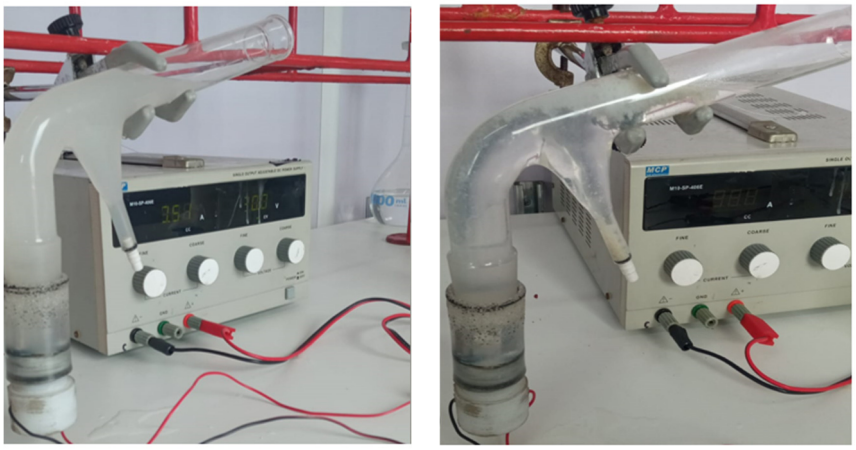

(**a**) (**b**)

Figure 5. Modified Hallimond tube, (**a**) before and (**b**) after the electroflotation process of clays.

Table 2. Operational and response parameters obtained for the electroflotation of clays using a modified Hallimond tube with an anode and cathode made of Ti Gr. 2.

Test	Clay Type	NaCl, M	t_{EF}, min	E_{cell}, V	I_{cell}, A (t = 0 min)	I_{cell}, A ($t = t_{EF}$)	$\%R_{MF}$
1	Montmorillonite	0.1	10	10	0.14	0.05	1.49
2		0.3	15	15	0.17	0.05	43.52
3		0.5	20	20	0.40	0.03	72.68
4	Kaolinite	0.1	10	10	0.15	0.03	2.37
5		0.3	15	15	0.23	0.04	45.72
6		0.5	20	20	0.80	0.03	88.44
7	Mix (1:1 wt%) Kao./Mont.	0.1	10	10	0.40	0.04	2.33
8		0.3	15	15	0.56	0.04	31.36
9		0.5	20	20	0.71	0.05	67.36

Although the cell current values decreased in magnitude (ranging between 0.03 and 0.05 A, equivalent to 68 and 114 A/m^2) compared to the beginning of the electroflotation process (t = 0 min), under the studied conditions (10, 15, and 20 V), water electrolysis was not unfavorable, and oxygen and hydrogen bubble generation was maintained over time. This confirms that cell current densities between 68 and 114 A/m^2 are sufficient for this process. This observation could be related to the increased passive film growth with high anodic oxygen bubble generation at the beginning of the process, where transitions in the crystalline phase of TiO_2 have occurred, which are caused by higher applied cell current densities [40,41]. However, the good corrosion resistance of TiO_2 passive film in saline environments can be compromised by the high cell voltage and current intensity, promoting the formation of titanium oxychlorides over the passive film by the action of chloride ions, according to the chemical reaction [29]:

$$Ti_xO_y + 2Cl^- \rightarrow Ti_xO_yCl_2 + 2e^- \quad (8)$$

Table 2 summarizes the electroflotation parameters for both kaolinite and montmorillonite and their mixtures under similar electroflotation times, cell voltages, and NaCl concentrations.

From Table 2, it is observed that for the three cases of clays (alone and mixtures), lower electrochemical conditions of time, cell voltage, and NaCl concentration promote lower electroflotation efficiencies between 1.4 and 2.5%. However, this efficiency parameter increases with the increase of the electrochemical conditions, reaching efficiencies higher to 65%. These results are directly related to the increase in the cell voltage, which increases the cell current, thus promoting a major generation of bubbles on the electrodes, in addition to an increase in the electroflotation time. Both parameters are related to Faraday's law. Moreover, it is also interesting to observe the effect of the NaCl concentration, which, although used to obtain a solution of high conductivity, would also promote corrosion on the electrodes. Under the optimal electroflotation conditions, the results show higher electroflotation efficiencies for kaolinite, reaching a value of 88.44%, compared to montmorillonite and the mixture of clays. These results are directly related to changes on the rheology and froth stability, where the swelling clays like montmorillonite accommodate large amounts of adsorbed water compared with non-swelling clays like kaolinite [42], adversely affecting the electroflotation performance. Additionally, these lower electroflotation efficiencies obtained for montmorillonite and the mixture of both clays are related to the increase in pulp viscosity, which, for example, increases from approximately 1 mPa·s for kaolinite to 8.8 mPa·s for montmorillonite under similar clay concentrations [43], thereby decreasing the electroflotation process.

Therefore, despite the relatively short duration of the electroflotation experiments, the results could be promising, reveling acceptable recovery rates of clays from electroflotation assays in saline environments such as solutions with salt concentrations equivalent to seawater. However, continuous evaluation of the system is essential to investigate potential variations in these parameters over longer electroflotation periods, as well as the influence of the multiple ions typically observed in seawater.

3.3. Electrochemical Behavior of Ti Gr. 2 in Presence of Clays

To quantitatively assess the corrosion behavior of Ti Gr. 2 electrodes in alkaline media and the presence of clays, electrochemical linear polarization curves were carried out. Figure 6 depicts polarization curves (Figure 6a) and Tafel curves (Figure 6b) obtained for Ti Gr. 2 immersed in 0.5 M NaCl in the absence and presence of clays. Additionally, the figure shows a comparison between experimental values (dotted lines) and fitted values (continuous lines) obtained by applying the superposition model according to Equation (2), given RMSE values of 3×10^{-3}, 8×10^{-4}, 3×10^{-3}, and 2×10^{-3}, for kaolinite, montmorillonite, 1:1 mixed clay, and pure NaCl solution, respectively. Table 3 summarizes the electrochemical and corrosion parameters determined for ORR, HER, and TOR by using Equations (3)–(5). The electrochemical results provide novel information related to the performance of Ti Gr. 2 used for both electrodes in contact with a 0.5 M NaCl solution with a suspension of kaolinite and montmorillonite clays. At potentials with more negatives than −800 mV/SHE [29,44], the HER, which dominates the current density, reveals an important reduction in the current density in the presence of clays compared with a pure solution of 0.5 M NaCl. Considering a fixed cathodic potential of −900 mV/SHE, the total current densities were 3.87, 5.53, and 9.24 A/m^2 for montmorillonite, kaolinite, and the mixture of both clays, respectively, which are low values compared with 15 A/m^2 for a solution in the absence of clays and containing only NaCl. These variations are in concordance with a smaller Tafel slope value for the test without clays, which also could be due to the adsorption of soluble species from clay samples, disfavoring the electrocatalytic capacity for hydrogen production from water electrolysis.

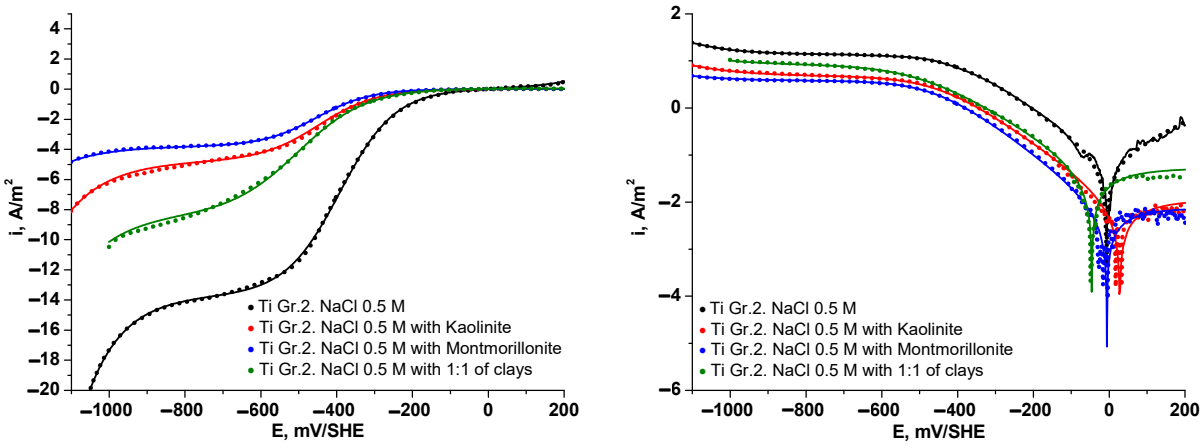

Figure 6. Polarization (**a**) and Tafel (**b**) curves for Ti Gr. 2 in contact with 0.5 M NaCl and slurry of clays. Experimental curve (dotted line) and fitted curve (line) obtained from the superposition model.

Table 3. Kinetic and corrosion parameters for Ti Gr. 2 electrode in NaCl and clay slurries, obtained from applying the superposition model.

Parameters	0.5M NaCl	0.5 M NaCl + (1:1) Kao./Mont.	0.5 M NaCl + 1000 ppm Kao.	0.5 M NaCl + 1000 ppm Mont.
$i_{0,Ti}$, A/m^2	1.99×10^{-9}	5.13×10^{-2}	9.60×10^{-3}	7.20×10^{-3}
t_{Ti}, mV/dec	238	231,629	159,369	243,684
i_{0,O_2}, A/m^2	-2.03×10^{-6}	-7.15×10^{-6}	-7.57×10^{-7}	-1.83×10^{-7}
t_{O_2}, mV/dec	−168	−207	−171	−165
i_{l,O_2}, A/m^2	−13.68	−8.38	−4.76	−3.79
i_{0,H_2}, A/m^2	-1.46×10^{-2}	-1.44×10^{-2}	-1.23×10^{-2}	-3.54×10^{-3}
t_{H_2}, mV/dec	−217	−247	−256	−253
E_{corr}, mV/SHE	−7	−48	27	−6
i_{corr}, A/m^2	0.0693	0.0522	0.0098	0.0073

Further, as expected, the entire cathodic branch for Ti Gr. 2 in 0.5 M NaCl was found to be higher compared with the presence of clays, which revealed lower current densities. The $i_{0,Ti}$ is significantly higher in the mixture of kaolinite and montmorillonite (1:1), indicating greater reactivity under this condition. In comparison, suspensions containing only kaolinite or montmorillonite exhibit much lower values, although still higher than that of the 0.5 M NaCl base solution. The mixture (1:1) also shows the highest i_{0,O_2}, suggesting an increase in electrochemical reactivity compared to suspensions containing only one type of clay. The $|t_{O_2}|$ is higher for the mixture (1:1) than other slurries and NaCl solutions, indicating a greater ease for the ORR to occur under these conditions. The i_{0,H_2} is similar between the base solution and the clay suspensions but is lower in solutions containing only kaolinite or montmorillonite, especially in the montmorillonite suspension. These results indicate a slight decrease in the kinetics under equilibrium conditions. The t_{H_2} is more negative in suspensions with kaolinite and montmorillonite, which could indicate a greater tendency for HER under these conditions.

Regarding the ORR, the polarization curves showed a good adjustment to a mixed kinetic by charge and mass transfer (see Equation (4)), where the limiting current density (i_{l,O_2}) trends to decrease in the presence of clays from 13.68 A/m^2 in NaCl solution to 3.8 A/m^2 in the presence of montmorillonite clay. These variations in i_{l,O_2} values for ORR represent a decay in the mass transfer of oxygen dissolved close to 28, 35, and 61% when the Ti Gr. 2 is in contact with slurries of montmorillonite, kaolinite, and the mix 1:1 of both clays, respectively, compared to a pure NaCl solution. The decreased oxygen mass transfer from bulk to metallic surface could be associated with changes in the density and viscosity

of the clay slurry, which are in turn consistent with the electroflotation recoveries for clays. Thus, it is possible to indicate that the values signify enhanced catalytic activity and greater efficiency in reducing molecular oxygen within a pure salt solution. Furthermore, the kinetic parameters show an interesting alteration when the Ti Gr. 2 is immersed in clays, which could be related to variations in the cell current during the electroflotation process.

As shown in Table 3, the Tafel slope for TOR in a NaCl solution has similar values commonly observed in the literature, ranging around 238 mV/dec [32]. As shown in Figure 6b, from the inversion potential towards anodic direction, the current density follows a planar tendency with the applied potential for tests in the presence of clays, compared to the tendency in a pure NaCl solution where the current density increases with the applied potential. This behavior, along with higher anodic Tafel slope values in the presence of clay slurries, indicates that the Ti Gr. 2 rapidly passivates with the formation of titanium oxides and promotes a good corrosion resistance [45]. Thus, based on this analysis, the exchange current density can be approximated to the passivation current density. The spontaneous passivation of the Ti Gr. 2 electrode is consistent with the current variations during the electroflotation tests. On the other hand, the cathodic kinetic parameter for ORR and HER does not show appreciable variations in clay slurries; however, these kinetic parameters were lower than that determined for a pure NaCl solution.

The variations of E_{corr} for clay slurries have not shown a clear tendency since that it was shifted to cathodic direction for the mixture (1:1) and to anodic direction for singles slurries with respect to E_{corr} for a pure NaCl solution. These variations are less than ±85 mV, which indicates that the clay slurry could affect both anodic and cathodic reactions [46], with a predominance effect on cathodic reactions for the mixture (1:1) slurry. The corrosion rate exhibited by the Ti Gr. 2 electrode in contact with a 0.5 M NaCl solution reveals convinced values of i_{corr} equal to 0.0693 A/m^2, compared to values obtained for the clays where lower corrosion rates were observed, and equals to 0.0098, 0.0073, and 0.0522 A/m^2 for kaolinite, montmorillonite, and the mix 1:1 of both clays, respectively. These results suggest that the salt suspension with montmorillonite has the best protection against corrosion under the studied conditions. Furthermore, the i_{corr} value obtained for a NaCl solution is comparable to Ti-Ni alloy electrodes in NaCl solution [47] and close to that observed qualitatively for Ti samples in NaCl solutions [48–50], where an inapplicability of the Tafel law was reported. These values are further supported by the performance of the Tafel curve depicted in Figure 6b, as well as the electrochemical kinetic parameters for both ORR, HER, and TOR presented in Table 3. The corrosion rates are directly related to the electroflotation efficiency, where, as shown in Tables 2 and 3, lower electroflotation efficiencies were found for higher corrosion rates. This could be attributed to a competition between anodic titanium oxidation with oxygen evolution reaction and the interference of soluble ions from clays and their further combination with hydroxyl anions in solution, such as $Al(OH)_3$ formation. This last effect, associated with the dissolved ions from clays, can be verified by comparing the corrosion rates and electroflotation efficiencies between kaolinite and montmorillonite clays with their dissolution rates [51,52], where a higher corrosion rate of the Ti Gr. 2 electrode in kaolinite slurry could be caused by a high Al/Si concentration relation (~0.85 at pH = 4 [51]), compared to the Ti Gr. 2 electrode in montmorillonite slurry, where a low corrosion rate is attributed to a lower Al/Si concentration relation (~0.42 at pH = 4 [52]).

Figure 7 delineates the behavior of the first derivative (di/dE) concerning instantaneous current variation with potential from the cathodic to the anodic direction. The following three discernible regions emerge: (i) Within the potential range of −1100 to −800 mV/SHE, the experimental and fitted results confirm that the charge transfer is the rate-determining step for HER, which is corroborated by higher obtained Tafel slope values ($|t_{H_2}| > 200$ mV/dec), revealing faster HER kinetics for the 0.5 M NaCl solution without clays; (ii) from −800 to −100 mV/SHE, the cathodic subprocess for ORR only shows a planar plateau between −800 and −650 mV/SHE followed by a symmetric distribution between −650 and −100 mV/SHE with a maximum inflection point, indicating that the

ORR is via a four-electron transfer pathway where a mixed control of charge and mass transfer is the rate-determining step, albeit decreasing the ORR kinetics in the presence of ultrafine clays in the saline solution; and (iii) from −100 to 200 mV/SHE, the derivative values reveal different tendencies in the NaCl solution without and with the presence of clays, where for kaolinite clay, the results confirm a spontaneous passivation of the Ti Gr. 2 electrode through the observations of the first derivative values with potential, contrary to the tendency observed for the 0.5 NaCl solution, which reveals an increase in the di/dE values with potential. Similar results were observed for montmorillonite clay and the 1:1 mixture of both studied clays.

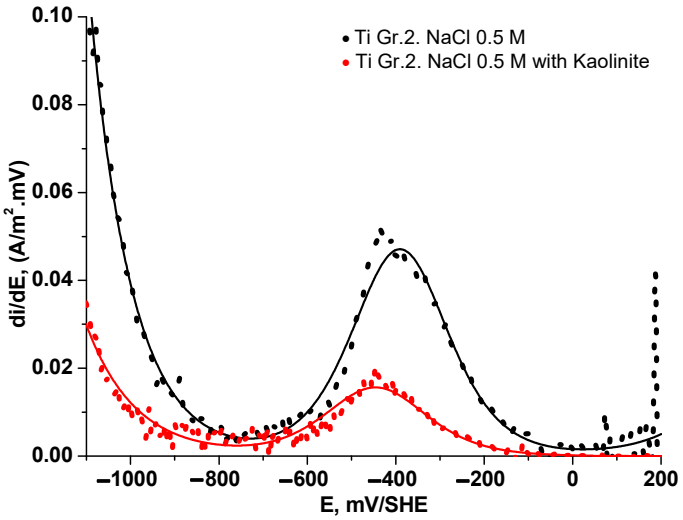

Figure 7. First derivative curve of current density-potential data for Ti Gr. 2 in 0.5 M NaCl and solution kaolinite slurry.

The electroflotation results for kaolinite, montmorillonite, and their 1:1 mixture, in conjunction with the kinetic and corrosion parameters for Ti Gr. 2 electrodes, provide novel insights into the concentration process of clays with particle sizes less than 32 µm in aggressive environments such as 0.5 M NaCl solution. Particularly, the kinetic parameters associated with the HER mechanism exhibit intriguing variability when the Ti Gr. 2 electrode interacts with different clay types. This suggests a direct influence of clay presence on the rate of HER at the cathodic electrode. Remarkably, the highest exchange current density is observed under operational conditions that closely mimic real-world scenarios encountered in mineral processing, specifically when operating with saline solutions containing clay mixtures. This heightened exchange current density signifies enhanced efficiency in the release or evolution of H_2 under such conditions. Similarly, the higher exchange current density for the ORR indicates rapid reaction processes occurring at the electrode–electrolyte interface, which is critical for the optimal performance of this electrochemical device.

To clarify the corrosion behavior of Ti Gr. 2 in NaCl solution, morphological inspection of the anode electrode after water electrolysis at 10 V in 0.5 M NaCl solution is shown in Figure 8. From this figure, it is evident corrosion on the metallic surface by the presence of some cracks on the oxide layer and small pitting sites. This corrosion damage can be the result of the presence of chloride ions in solutions, promoting localized corrosion.

The use of Ti Gr. 2 in this experiment, as well as in others, is due to the fact that electrochemical devices, such as electroclorination systems for OCl^- production, typically utilize titanium as both the cathode and anode. Electroflotation in saline media is a novel process that has not been scaled up for industrial applications. In this context, it is crucial to understand the electrochemical behavior of typical materials used in saline environments to ensure their sustainability for industrial uses.

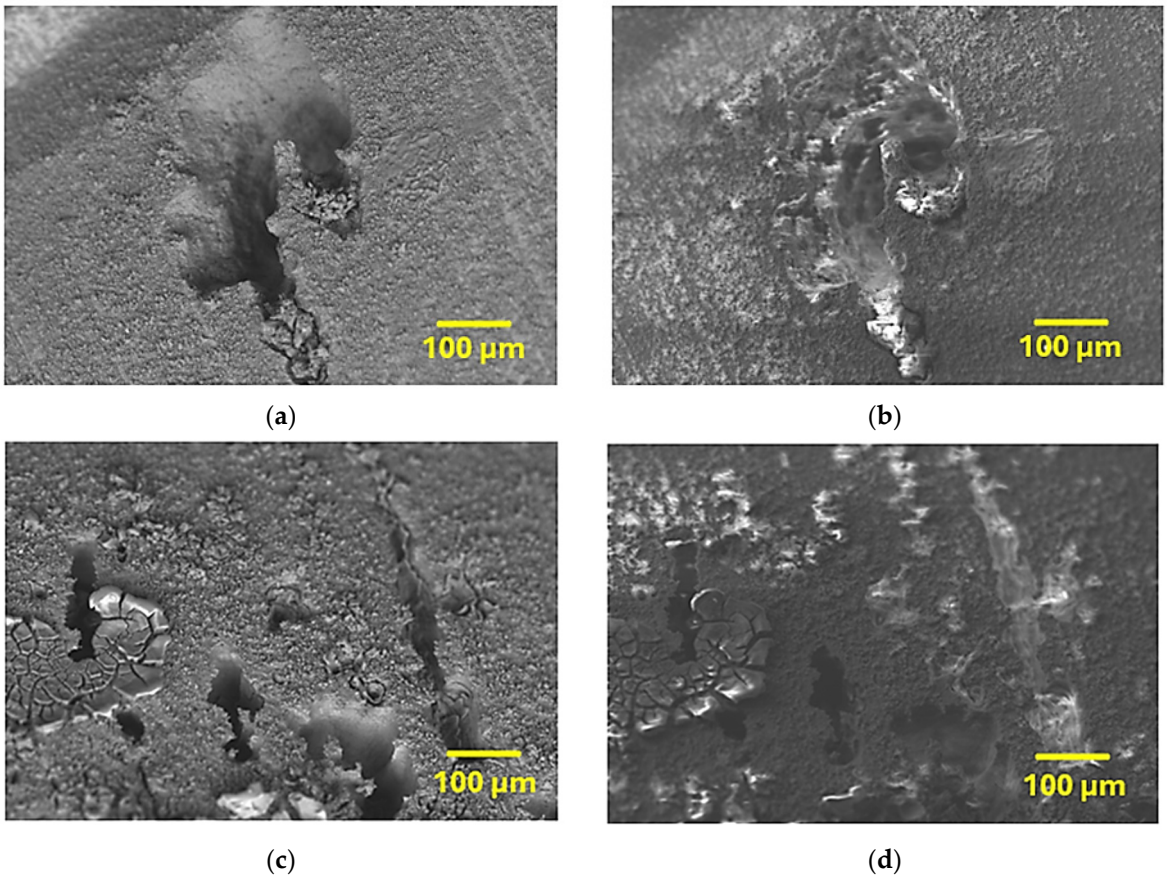

(**a**) (**b**)

(**c**) (**d**)

Figure 8. Pitting corrosion (**a**,**b**), and cracks on the oxide layer (**c**,**d**) detected over the Ti anode at 10 V operating for 1 h in 0.5 M NaCl.

In this study, the exchange current density for HER and ORR in individual kaolinite and montmorillonite slurries was found to be lower than those observed with the clay mixture slurry. This implies that the kinetics achieved with the clay mixture could be an optimal condition for the cathodic subprocess operation. A higher exchange current density can significantly enhance operational efficiency, leading to improved long-term stability.

Furthermore, as indicated previously, the high values of the Tafel slope for HER suggest the adsorption of intermediate products, which could represent the rate-limiting step of the reaction, resulting in a slower response to changes in applied potential without altering the bubble size. However, when conducting experiments with real clays and their impurities, the Tafel slope values can be drastically affected. This is primarily due to their influence on (i) the rate of electron transfer and (ii) the concentration of hydrogen protons. These factors can significantly modify the kinetics of the HER, leading to variations in the observed Tafel slope.

4. Conclusions

The electrochemical performance of Ti Gr. 2 as electrodes for the electroflotation process of individual kaolinite and montmorillonite clay, as well as their 1:1 mixture in a 0.5 M NaCl solution, was studied. The electroflotation recovery and corrosion behavior of Ti Gr. 2 were investigated using a modified Hallimond tube and the superposition model, respectively. An increase in cell voltage and current leads to an increase in the electroflotation recovery, with maximum recovery rates of 72.68, 88.44, and 67.36% for montmorillonite, kaolinite, and their 1:1 mixture, respectively. The electrochemical behavior of Ti Gr. 2 exhibited a high dependence on the presence of clay slurries, where passivation behavior and a decrease in the kinetics of ORR and HER were observed for the anodic and cathodic reactions, respectively. The corrosion rate in a chloride solution without clays was

0.0693 A/m^2, whereas the rates in the presence of chloride with clays were lower, reaching values of 0.0098 A/m^2 for kaolinite, 0.0073 A/m^2 for montmorillonite, and 0.0522 A/m^2 for the 1:1 mixture of both clays. These findings will serve to complement material analyses and optimize the electroflotation process, which has revealed a good application in highly saline environments such as seawater.

Author Contributions: Conceptualization, F.M.G.-M., A.S. and B.A.-F.; methodology, S.S.-A. and S.A.; software, A.S. and A.G.; validation, F.M.G.-M., A.S. and J.Á.C.-M.; formal analysis, F.M.G.-M., A.S. and B.A.-F.; investigation, J.Á.C.-M., S.S.-A. and S.A.; resources, F.M.G.-M. and B.A.-F.; data curation, A.S. and A.G.; writing—original draft preparation, F.M.G.-M. and A.S.; writing—review and editing, J.Á.C.-M., A.G., A.S. and F.M.G.-M.; supervision, A.S. and F.M.G.-M. All authors have read and agreed to the published version of the manuscript.

Funding: This research received no external funding.

Institutional Review Board Statement: Not applicable.

Informed Consent Statement: Not applicable.

Data Availability Statement: The data presented in this manuscript are available upon request from the corresponding author.

Acknowledgments: The authors would like to thank the Programa de Doctorado en Energía Solar of the Universidad de Antofagasta, Chile; the support of ANID-Chile through the research project FONDECYT Iniciación 11230550; the Project DIUDA N° 22430 carried out by the Facultad de Ingeniería of the Universidad de Atacama; and ANID/FONDAP 1522A0006 Solar Energy Research Center SERC-Chile. The authors would like to thank C. Portillo for their technical support.

Conflicts of Interest: The authors declare no conflicts of interest.

References

1. Shao, D.; Li, X.; Gu, W. A Method for Temporary Water Scarcity Analysis in Humid Region Under Droughts Condition. *Water Resour. Manag.* **2015**, *29*, 3823–3839. [CrossRef]
2. Fernandez-Scagliusi, M.Á. Herramientas para lograr un uso sostenible del agua en la minería: La huella hídrica y la huella de agua. *Rev. Catalana Dret Ambient.* **2021**, *12*, 10. [CrossRef]
3. Cisternas, L.A.; Gálvez, E.D. The use of seawater in mining. *Min. Proc. Ext. Met. Rev.* **2018**, *39*, 18–33. [CrossRef]
4. COCHILCO. Yearbook: Copper and Other Mineral statistics 2003–2022. 2022. Available online: https://www.cochilco.cl/Lists/Anuario/Attachments/27/ANUARIO_ESTADISTICO_COCHILCO%20A%C3%91O%202022.pdf (accessed on 24 May 2024).
5. Witecki, K.; Polowczyk, I.; Kowalczuk, P. Chemistry of wastewater circuits in mineral processing industry—A review. *J. Water Process Eng.* **2022**, *45*, 102509. [CrossRef]
6. Zhang, N.; Chen, X.; Peng, Y. The interaction between kaolinite and saline water in affecting the microstructure, rheology and settling of coal flotation products. *Powder Technol.* **2020**, *372*, 76–83. [CrossRef]
7. Gorakhki, M.H.; Bareither, C.A. Salinity effects on sedimentation behavior of kaolin, bentonite, and soda ash mine tailings. *Appl. Clay Sci.* **2015**, *114*, 593–602. [CrossRef]
8. Rand, B.; Melton, I.E. Particle interactions in aqueous kaolinite suspensions. I. Effect of pH and electrolyte upon the mode of particle interaction in homoionic sodium kaolinite suspensions. *J. Colloid Interface Sci.* **1977**, *60*, 308–320. [CrossRef]
9. Yaghmaeiyan, N.; Mirzaei, M.; Delghavi, R. Montmorillonite clay: Introduction and evaluation of its applications in different organic syntheses as catalyst: A review. *Results Chem.* **2022**, *4*, 100549. [CrossRef]
10. Romanov, A.M. Electroflotation in Waste Water Treatment: Results and Perspectives. In *Mineral Processing and the Environment*; Springer: Berlin/Heidelberg, Germany, 1998; pp. 335–360.
11. Srinivasan, V.; Subbaiyan, M. Electroflotation Studies on Cu, Ni, Zn, and Cd with Ammonium Dodecyl Dithiocarbamate. *Sep. Sci. Technol.* **1989**, *24*, 145–150. [CrossRef]
12. Alexandrova, L.; Nedialkova, T.; Nishkov, I. Electroflotation of Metal Ions in Waste Water. *Int. J. Miner. Process.* **1994**, *41*, 285–294. [CrossRef]
13. Oussedik, S.M.; Khelifa, A. Reduction of Copper Ions Concentration in Wastewaters of Galvanoplastic Industry by Electroflotation. *Desalination* **2001**, *139*, 383. [CrossRef]
14. Khelifa, A.; Moulay, S.; Naceur, A.W. Treatment of Metal Finishing Effluents by the Electroflotation Technique. *Desalination* **2005**, *181*, 27–33. [CrossRef]
15. Merzouk, B.; Gourich, B.; Sekki, A.; Madani, K.; Chibane, M. Removal Turbidity and Separation of Heavy Metals Using Electrocoagulation-Electroflotation Technique. A Case Study. *J. Hazard Mater.* **2009**, *164*, 215–222. [CrossRef]

16. Zouboulis, A.I.; Matis, K.A. Cadmium Ion Removal by Electroflotation onto Sewage Sludge Biomass. *Int. J. Environ. Waste Manag.* **2012**, *9*, 245–256. [CrossRef]
17. Madrid, F.M.G.; Arancibia-Bravo, M.P.; Sepúlveda, F.D.; Lucay, F.A.; Soliz, A.; Cáceres, L. Ultrafine Kaolinite Removal in Recycled Water from the Overflow of Thickener Using Electroflotation: A Novel Application of Saline Water Splitting in Mineral Processing. *Molecules* **2023**, *28*, 3954. [CrossRef]
18. Kyzas, G.Z.; Matis, K.A. Electroflotation Process: A Review. *J. Mol. Liq.* **2016**, *220*, 657–664. [CrossRef]
19. Kydros, K.A.; Gallios, G.P.; Matis, K.A. Electrolytic Flotation of Pyrite. *J. Chem. Technol. Biotechnol.* **1994**, *59*, 223–232. [CrossRef]
20. Bhaskar Raju, G.; Khangaonkar, P.R. Electro-Flotation of Chalcopyrite Fines. *Int. J. Miner. Process.* **1982**, *9*, 133–143. [CrossRef]
21. Makuei, F.; Tadesse, B.; Albijanic, B.; Browner, R. Electroflotation of Ultrafine Chalcopyrite Particles with Sodium Oleate Collector. *Miner. Eng.* **2018**, *120*, 44–46. [CrossRef]
22. Hacha, R.R.; LeonardoTorem, M.; Gutiérrez Merma, A.; da Silva Coelho, V.F. Electroflotation of Fine Hematite Particles with Rhodococcus Opacus as a Biocollector in a Modified Partridge–Smith Cell. *Miner. Eng.* **2018**, *126*, 105–115. [CrossRef]
23. Llerena, C.; Ho, J.C.K.; Piron, D.L. Effects of pH on Electroflotation of Sphalerite. *Chem. Eng. Commun.* **1996**, *155*, 217–228. [CrossRef]
24. Liu, A.; Fan, P.; Han, F.; Han, H.; Li, Z.; Wang, H.; Fan, M. Effect of Electroflotation on Quartz and Magnetite and Its Utilization on the Reverse Flotation of Magnetic Separation Concentrate. *Miner. Eng.* **2022**, *175*, 107292. [CrossRef]
25. Tadesse, B.; Albijanic, B.; Makuei, F.; Browner, R. Recovery of Fine and Ultrafine Mineral Particles by Electroflotation—A Review. *Miner. Process. Extr. Metall. Rev.* **2019**, *40*, 108–122. [CrossRef]
26. Hacha, R.R.; Merma, A.G.; Couto, H.J.B.; Torem, M.L. Measurement and analysis of H_2 and O_2 bubbles diameter produced by electroflotation processes in a modified Partridge-Smith cell. *Powder Technol.* **2019**, *342*, 308–320. [CrossRef]
27. Alam, R.; Shang, J.Q.; Khan, A.H. Bubble size distribution in a laboratory-scale electroflotation study. *Environ. Monit. Assess.* **2017**, *189*, 193. [CrossRef] [PubMed]
28. Mraz, R.; Krysa, J. Dimensionally Stables Anodes with a Long Lifetime for Electroflotation. In *Precision Process Technology*; Springer: Berlin/Heidelberg, Germany, 1993; pp. 681–688.
29. El-Ghenymy, A.; Alsheyab, M.; Khodary, A.; Sirés, I.; Abdel-Wahab, A. Corrosion Behavior of Pure Titanium Anodes in Saline Medium and Their Performance for Humic Acid Removal by Electrocoagulation. *Chemosphere* **2020**, *246*, 125674. [CrossRef] [PubMed]
30. Wang, Z.B.; Hu, H.X.; Liu, C.B.; Zheng, Y.G. The effect of fluoride ions on the corrosion behavior of pure titanium in 0.05 M sulfuric acid. *Electrochim. Acta* **2014**, *135*, 526–535. [CrossRef]
31. Pei, D.-N.; Gong, L.; Zhang, A.-Y.; Zhang, X.; Chen, J.-J.; Mu, Y.; Yu, H.-Q. Defective titanium dioxide single crystals exposed by high-energy {001} facets for efficient oxygen reduction. *Nat. Commun.* **2015**, *6*, 8696. [CrossRef]
32. Madrid, F.M.G.; Arancibia-Bravo, M.; Cisterna, J.; Soliz, Á.; Salazar-Avalos, S.; Guevara, B.; Sepúlveda, F.; Cáceres, L. Corrosion of Titanium Electrode Used for Solar Saline Electroflotation. *Materials* **2023**, *16*, 3514. [CrossRef]
33. Kelly, E.J.; Bronstein, H.R. Kinetics and Mechanism of the Hydrogen Evolution Reaction on Titanium in Acidic Media. *J. Electrochem. Soc.* **1984**, *131*, 2232–2238. [CrossRef]
34. Chen, C.C.; Chen, J.H.; Chao, C.G.; Say, W.C. Electrochemical characteristics of surface of titanium formed by electrolytic polishing and anodizing. *J. Mater. Sci.* **2005**, *40*, 4053–4059. [CrossRef]
35. Soliz, A.; Cáceres, L. Corrosion behavior of carbon steel in LiBr in comparison to NaCl solutions under controlled hydrodynamic conditions. *Int. J. Electrochem. Sci.* **2015**, *10*, 5673–5693. [CrossRef]
36. Wang, Y.; Fugetsu, B.; Sakata, I.; Fujisue, C.; Kabayama, S.; Tahara, N.; Morisawa, S. Monolayered Platinum Nanoparticles as Efficient Electrocatalysts for the Mass Production of Electrolyzed Hydrogen Water. *Sci. Rep.* **2020**, *10*, 10126. [CrossRef] [PubMed]
37. Soliz, A.; Cáceres, L.; Pineda, F.; Galleguillos, F. Erosion–Corrosion of AISI 304L Stainless Steel Affected by Industrial Copper Tailings. *Metals* **2020**, *10*, 1005. [CrossRef]
38. Werling, N.; Kaltenbach, J.; Weidler, P.G.; Schuhmann, R.; Dehn, F.; Emmerich, K. Solubility of calcined kaolinite, montmorillonite, and illite in high molar NaOH and suitability as precursors for geopolymers. *Clays Clay Miner.* **2022**, *70*, 270–289. [CrossRef]
39. Zhong, Y.; Yang, Q.; Li, X.; Yao, F.; Xie, L.; Zhao, J.; Chen, F.; Xie, T.; Zeng, G. Electrochemically Induced Pitting Corrosion of Ti Anode: Application to the Indirect Reduction of Bromate. *Chem. Eng. J.* **2016**, *289*, 114–122. [CrossRef]
40. Xing, J.H.; Xia, Z.B.; Hu, J.F.; Zhang, Y.H.; Zhong, L. Time dependence of growth and crystallization of anodic titanium oxide films in potentiostatic mode. *Corros. Sci.* **2013**, *75*, 212–219. [CrossRef]
41. Liu, Z.; Liu, X.; Donatus, U.; Thompson, G.E.; Skeldon, P. Corrosion behaviour of the anodic oxide film on commercially pure titanium in NaCl environment. *Int. J. Electrochem. Sci.* **2014**, *9*, 3558–3573. [CrossRef]
42. Hatch, C.D.; Wiese, J.S.; Crane, C.C.; Harris, K.J.; Kloss, H.G.; Baltrusaitis, J. Water Adsorption on Clay Minerals as a Function of Relative Humidity: Application of BET and Freundlich Adsorption Models. *Langmuir* **2012**, *28*, 1790–1803. [CrossRef]
43. Chen, L.; Zhao, Y.; Bai, H.; Ai, Z.; Chen, P.; Hu, Y.; Song, S.; Komarneni, S. Role of Montmorillonite, Kaolinite, or Illite in Pyrite Flotation: Differences in Clay Behavior Based on Their Structures. *Langmuir* **2020**, *36*, 10860–10867. [CrossRef]
44. Qiao, Y.; Qin, Y.; Zhou, H.; Yang, L.; Wang, X.; Wang, Z.; Liu, Z.; Zou, J. Electrochemical hydrogen charging on corrosion behavior of Ti-6Al-4V alloy in artificial seawater. *Chin. J. Mech. Eng.* **2024**, *37*, 2. [CrossRef]
45. Xue, C.; Zhang, P.; Wei, D.; Hu, H.; Li, F.; Yang, K. Corrosion and Tribocorrosion Behaviors for TA3 in Ringer's Solution after Implantation of Nb Ions. *Appl. Sci.* **2020**, *10*, 8329. [CrossRef]

46. Talat, R.; Asghar, M.A.; Liaqat, F.; Satti, M.; Fatima, S.; Haider, A.; Ali, S. Adsorption and anticorrosion studies of newly designed Schiff bases for the protection of EN3B mild steel in 3.5% NaCl solution: A combined experimental and theoretical approach. *J. Mol. Liq.* **2023**, *388*, 122776. [CrossRef]
47. Lazić, M.M.; Mitić, D.; Radović, K.; Đorđević, I.; Majerič, P.; Rudolf, R.; Grgur, B.N. Corrosion Behavior of Nickel–Titanium Continuous-Casted Alloys. *Metals* **2024**, *14*, 88. [CrossRef]
48. Kostelac, L.; Pezzato, L.; Colusso, E.; Natile, M.M.; Brunelli, K.; Dabalà, M. Black PEO Coatings on Titanium and Titanium Alloys Produced at Low Current Densities. *Appl. Sci.* **2023**, *13*, 12280. [CrossRef]
49. Tiwari, A.K.; Singh, R.K.; Ji, G. Investigation on corrosion behaviour of electrical discharge machined surfaces of Titanium-C2 in NaCl solution. *Mater. Today Proc.* 2023, *in press*. [CrossRef]
50. Fekry, A.M. The Influence of Chloride and Sulphate Ions on the Corrosion Behavior of Ti and Ti-6Al-4V Alloy in Oxalic Acid. *Electrochim. Acta* **2009**, *54*, 3480–3489. [CrossRef]
51. Ganor, J.; Mogollón, J.L.; Lasaga, A.C. The effect of pH on kaolinite dissolution rates and on activation energy. *Geochim. Et. Cosmochim. Acta* **1995**, *59*, 1037–1052. [CrossRef]
52. Rozalén, M.L.; Huertas, F.J.; Brady, P.V.; Cama, J.; García-Palma, S.; Linares, J. Experimental study of the effect of pH on the kinetics of montmorillonite dissolution at 25 °C. *Geochim. Cosmochim. Acta* **2008**, *72*, 4224–4253. [CrossRef]